

Shock Waves - An International Journal on Shock Waves, Detonations and Explosions

EXPERIMENTS AND ANALYSIS OF WATER-SHEET BREAKUP AND MITIGATING POTENTIAL UNDER BLAST LOADING

--Manuscript Draft--

Manuscript Number:	
Full Title:	EXPERIMENTS AND ANALYSIS OF WATER-SHEET BREAKUP AND MITIGATING POTENTIAL UNDER BLAST LOADING
Article Type:	Original paper
Keywords:	Water blast mitigation; water-sheet; explosively driven shock tube; protective water barrier.
Corresponding Author:	Steven F. Son, PhD Purdue University West Lafayette, IN UNITED STATES
Corresponding Author Secondary Information:	
Corresponding Author's Institution:	Purdue University
Corresponding Author's Secondary Institution:	
First Author:	Andrew James Zakrajsek, MSME
First Author Secondary Information:	
Order of Authors:	Andrew James Zakrajsek, MSME Daniel R. Guildenbecher, PhD Steven F. Son, PhD
Order of Authors Secondary Information:	
Abstract:	<p>An explosion yielding a blast wave can cause catastrophic damage to people and property. To mitigate damage from such an event, a number of investigators have proposed the use of water in various configurations. In this investigation, an unconfined free-flowing water-sheet, with an approximate thickness of 0.3 cm, is experimentally examined using an explosively driven shock tube at three different standoff distances. The results show that the water-sheet mitigates the initial peak overpressure and impulse of the blast. Further insights into the underlying physics are revealed by a numerical simulation using Sandia's CTH hydrocode. In simulations and experiments, the air behind the water sheet experiences two distinct pressure peaks. An initial pressure rise results from the passage of a low pressure shock wave ($M \approx 1$) through the intact sheet and into the air downstream of the water sheet. Following this, the water sheet breaks apart due to an increase in pressure on the forward surface caused by the buildup of the subsonic detonation products. Passage of the detonation products after breakup results in a second rise in pressure behind the water-sheet. In simulations, an initial perturbation of the water sheet is shown to affect the breakup time significantly. Additional simulations show that increasing the sheet thickness tends to increase the shock wave mitigation. These results indicate that it may be possible to optimize the thickness and surface morphology of a water-sheet to effectively mitigate damage due to explosive blast waves.</p>
Suggested Reviewers:	Jeffrey W. Jacobs, PhD Department Head, Elwin G. Wood Distinguished Professor, University of Arizona jwjacobs@email.arizona.edu Relevant experience in field Arun Shukla, PhD Simon Ostrach Professor, University of Rhode Island shuklaa@egr.uri.edu

	<p>Relevant experience in field</p>
	<p>Riccardo Bonazza, PhD Professor , University of Wisconsin-Madison bonazza@engr.wisc.edu Relevant research paper and work in the field</p>
	<p>Lee Glascoe , PhD Researcher , Lawrence Livermore National Laboratory (LLNL) Glascoe1@llnl.gov Relevant work with - Underwater Blast Experiments and Modeling for Shock Mitigation</p>
	<p>Melvin R. Baer, PhD Sandia National Lab mrbaer@sandia.gov Relevant work with shock mitigation in dense particle field</p>

EXPERIMENTS AND ANALYSIS OF WATER-SHEET BREAKUP AND MITIGATING POTENTIAL UNDER BLAST LOADING

A. J. Zakrajsek¹, D. R. Guildenbecher^{1,2}, and S. F. Son¹

¹*School of Mechanical Engineering, Purdue University, West Lafayette IN 47907*

²*Present Address: Sandia National Laboratories, Albuquerque NM 87123*

Abstract An explosion yielding a blast wave can cause catastrophic damage to people and property. To mitigate damage from such an event, a number of investigators have proposed the use of water in various configurations. In this investigation, an unconfined free-flowing water-sheet, with an approximate thickness of 0.3 cm, is experimentally examined using an explosively driven shock tube at three different standoff distances. The results show that the water-sheet mitigates the initial peak overpressure and impulse of the blast. Further insights into the underlying physics are revealed by a numerical simulation using Sandia's CTH hydrocode. In simulations and experiments, the air behind the water sheet experiences two distinct pressure peaks. An initial pressure rise results from the passage of a low pressure shock wave ($M \approx 1$) through the intact sheet and into the air downstream of the water sheet. Following this, the water sheet breaks apart due to an increase in pressure on the forward surface caused by the buildup of the subsonic detonation products. Passage of the detonation products after breakup results in a second rise in pressure behind the water-sheet. In simulations, an initial perturbation of the water sheet is shown to affect the breakup time significantly. Additional simulations show that increasing the sheet thickness tends to increase the shock wave mitigation. These results indicate that it may be possible to optimize the thickness and surface morphology of a water-sheet to effectively mitigate damage due to explosive blast waves.

Keywords: *Water blast mitigation, water-sheet, explosively driven shock tube, protective water barrier.*

Corresponding Author: Steven F. Son

Zucrow Laboratories - Chaffee Hall 130
500 Allison Rd. West Lafayette, IN 47907
sson@purdue.edu
Office Number: 765-494-8208
Fax Number: 765-494-0530

1 Introduction

Since 1968, bombings have accounted for nearly half of international terrorist attacks [1]. To counter these threats, defensive mechanisms, such as blast mitigants, are needed to protect structures and individuals from blast waves. Because it is often readily available, water is an attractive material for use as a blast mitigant [2]. Previous investigations have focused on blast mitigation by water sprays or confined masses of water [2, 3] with mixed success as quantified by the peak overpressure and impulse mitigation. An alternative geometry is that of a free-flowing water-sheet forming a shield around the object to be protected. A few numerical models have considered this geometry [4, 5], and their results indicate that water-sheets may effectively limit the peak overpressure of the blast. However, there are limited experimental data to validate these findings. Meekunnasombat *et al.* [6] considered liquid layers in a confined vertical shock tube, and their experiments highlighted the advantageous behavior of multiple layers of water. However, it is unclear if their results can be extended to the case of the unconfined water-sheet, which is the likely geometry for practical blast mitigation. In addition, Bremond and Villermaux [7] considered the breakup of a thin soap film under normally incident shock loading. However, it is unclear if the physical breakup mechanisms revealed in their investigation can be extended to the thicker water-sheets considered here.

The aim of this work is to study the blast mitigating potential associated with a sheet of water. To elucidate the fundamental physics, an experimental investigation is coupled with a numerical model. Sections 2 and 3 focus on the experimental configuration and results, respectively. Numerical results are presented in Section 4. The results presented here form an initial starting point to determine the feasibility of water-sheets as a possible blast mitigant.

2 Experimental configuration

2.1 Explosively driven shock tube

Experiments are conducted in an open field, with an explosively driven shock tube, and a custom fabricated water-sheet generator. A schematic of the experimental configuration is shown in Fig. 1. The explosively driven shock tube is used to produce a relevant laboratory size blast wave. Previous work has shown that this configuration yields a blast profile similar to open field explosive tests, and the shock tube directs the energy from the blast in one direction allowing for the use of less explosive as compared to a conventional open field explosive test [8, 9].

In an experiment, the explosively driven shock tube is loaded with 3 grams of Primasheet 1000. Primasheet 1000 is a pentaerythritol tetranitrate (PETN) based plastic explosive consisting of approximately 63% PETN powder [9]. Initiation of the PETN plastic sheet explosive is achieved by a combination of detonation cord (PETN powder) and an explosive bridge wire (EBW) detonator (RP-502 EBW) charged by a firing set.

The shock tube consists of a detonation chamber and a high explosive chamber. The two chambers are bolted together to protect the cables, test apparatus, and other equipment from the fragments produced by the aluminum detonator cap. A small hole links the two chambers and allows for passage of detonation cord. By changing the distance of the shock tube from the water-sheet (defined as the *standoff distance*), the characteristics of the incident shock wave are altered. Decreasing the standoff distance increases the overpressure at the water-sheet.

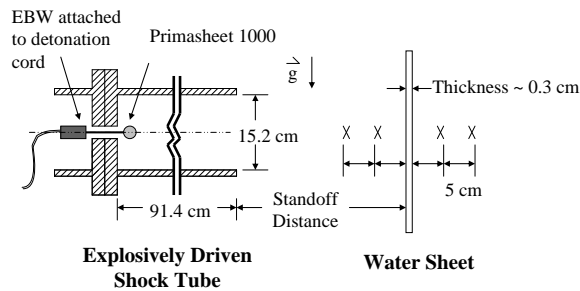


Fig. 1 Experimental configuration for investigation of blast loading of an unconfined water-sheet. The out of plane water-sheet dimension is roughly 70 cm, while the in plane height is 30 cm. The “X’s” indicate the location of the static pressure gauges which are positioned along the centerline of the shock tube.

2.2 Water-sheet generator and pressure gauges

A water-sheet is generated with a custom fabricated water-sheet generator, operating at a constant flow rate of approximately 56 L/min, producing a sheet approximately 0.3 cm thick. In the absence of blast loading, the water-sheet is continuous and displays surface perturbations, which likely arise from turbulent or capillary instabilities. In an experiment, the incoming blast wave is approximately normal to the water-sheet.

Due to space constraints near the water-sheet, typical pencil gauges cannot be placed at the locations marked in Fig. 1 without disrupting the water flow. Instead, PCB 113A22/113B22 piezoelectric dynamic pressure sensors are threaded into custom fabricated plates orientated to measure the static pressure of the blast. The experimental configuration includes two pressure gauges placed in front and two behind the water-sheet, as shown in Fig 1. As the water-sheet standoff distance is varied from one experiment to the next, the pressure gauges are repositioned to maintain the distances with respect to the water-sheet shown in Fig. 1.

2.3 Shadowgraphy visualization

In select experiments, the shock wave is visualized using the high-speed shadowgraphy technique described in [10]. Videos are recorded at 11,494 fps and an exposure of 26 μ s using a Vision Research Phantom v7.3 digital high-speed camera and an Oriel 1000 W xenon arc lamp. The field of view is approximately 53 by 53 cm and is recorded on a 171 by 171 pixel region of the CCD.

3 Experimental results

Experiments were performed at three different standoff distances: 20 cm, 31 cm, and 41 cm (distance from exit of shock tube to water sheet). To verify repeatability, all experiments were performed three times.

3.1 Pressure measurements

Figure 2 shows the free field pressure traces taken without the water sheet. Additionally, tabulated values for all free field distances measured are shown in Table 1. Figure 3 displays the pressure traces from an experiment with a water-sheet at a 31 cm standoff distance. Note the significantly lower peak pressures at distances behind the water sheet (36 and 41 cm). Other standoff distances produce similar results. Table 2 summarizes the pressure measurements after

the water sheets, for all three standoff distances considered. In this table, the peak overpressure is taken as the highest recorded static pressure during the transient experiment. The standard error is calculated between the three experiments performed at each condition.

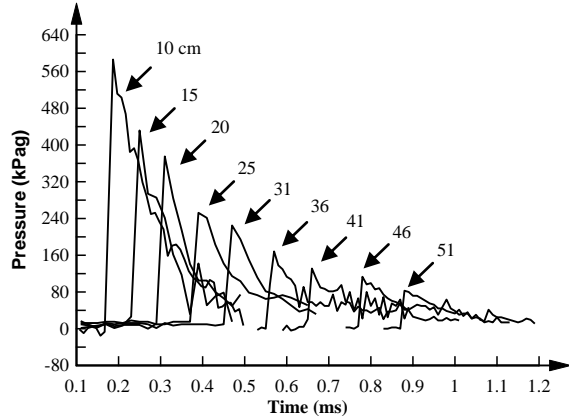


Fig. 2 Free field experimental pressure traces. Numbers indicate the distances in cm between the exit of the shock tube and the pressure gauge.

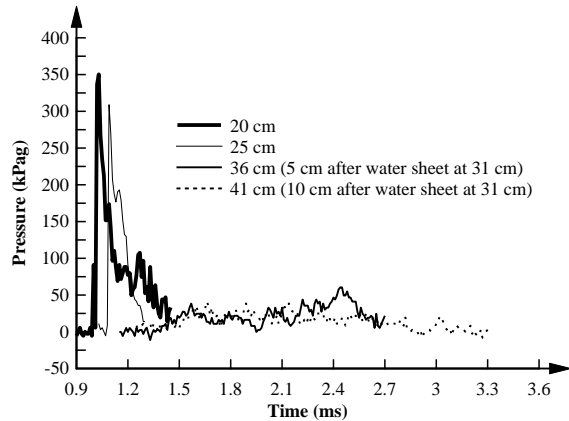


Fig. 3 Pressure trace of a blast test with a water-sheet at a 31 cm standoff distance. Numbers indicate the distances in cm between the exit of the shock tube and the pressure gauge.

Table 1 Free field experimental shock wave parameters. Uncertainties indicate the standard error.

Pressure Gauge Standoff Distance (cm)	Peak Overpressure (kPa)	Impulse (kPa-ms)	Positive Pulse (ms)
10	586 ± 29	60 ± 9	0.2 ± 0.1
15	436 ± 18	35 ± 8	0.2 ± 0.1
20	389 ± 15	32 ± 5	0.3 ± 0.1
25	253 ± 21	32 ± 3	0.3 ± 0.1
31	203 ± 19	19 ± 5	0.2 ± 0.1
36	169 ± 3	19 ± 4	0.3 ± 0.1
41	130 ± 1	18 ± 2	0.3 ± 0.1
46	117 ± 4	18 ± 1	0.4 ± 0.1
51	88 ± 6	12 ± 1	0.3 ± 0.1

Table 2 Initial experimental shock wave parameters 5 and 10 cm after the water sheets. Uncertainties indicate the standard error.

Water Sheet Standoff Distance (cm)	5 cm after Water Sheet		
	Peak Overpressure (kPa)	Impulse (kPa-ms)	Positive Pulse (ms)
20	60 ± 8	18 ± 3	0.3 ± 0.1
31	31 ± 4	5 ± 2	0.3 ± 0.1
41	26 ± 5	6 ± 2	0.4 ± 0.1
Water Sheet Standoff Distance (cm)	10 cm after Water Sheet		
	Peak Overpressure (kPa)	Impulse (kPa-ms)	Positive Pulse (ms)
20	53 ± 6	12 ± 3	0.3 ± 0.1
31	27 ± 8	4 ± 0.3	0.3 ± 0.1
41	23 ± 3	6 ± 0.4	0.4 ± 0.1

3.2 Pressure trace after water sheet

The experimental results show that the unconstrained free flowing water-sheet significantly reduces the initial overpressure and impulse of the blast. This is best illustrated in Fig. 3. At the 31 cm water-sheet standoff distance the peak overpressure is reduced by 82% and the impulse is reduced by nearly 75% as measured by the pressure gage placed 5 cm behind the water sheet. These results show qualitative agreement with previous work with water shields [4, 5].

The pressures measured downstream of the water-sheet also show a somewhat unexpected increase in the pressure at a finite time following the passage of the initial shock wave. Some pressure traces showed this rise in the pressure more distinctly. Figure 4 highlights the pressures measured downstream of the water-sheet at 31 cm. Based on the distances between the measurement points and the delay time between the initial pressure rise, it is found that the initial transmitted wave propagates at approximately sonic conditions. The second pressure increase, which occurs sometime after the passage of the sonic wave, is a subsonic pressure wave and is likely result of the detonation products which reach the downstream pressure gauges after the water-sheet breaks apart.

The breakup time of the water-sheet is estimated from the pressure recordings and is defined as the elapsed time between the instant when the shock wave reaches the water-sheet and the second rise in pressure, which is assumed to be due to passage of the detonation products. The experimental breakup times are shown in Fig. 5, which indicates that the water-sheet breakup time decreases with increasing incident shock pressure.

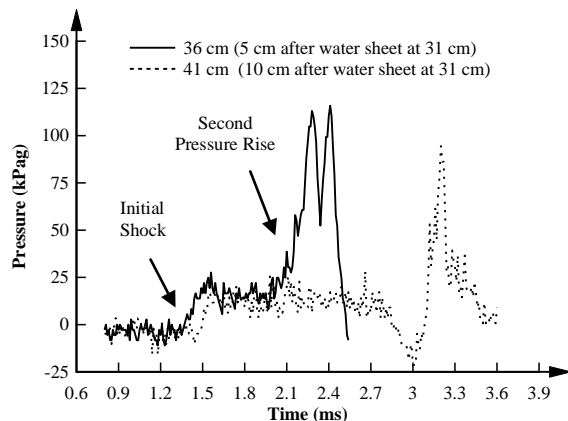


Fig. 4 Pressure trace of gauges 5 and 10 cm behind the water-sheet at a 31 cm standoff distance.

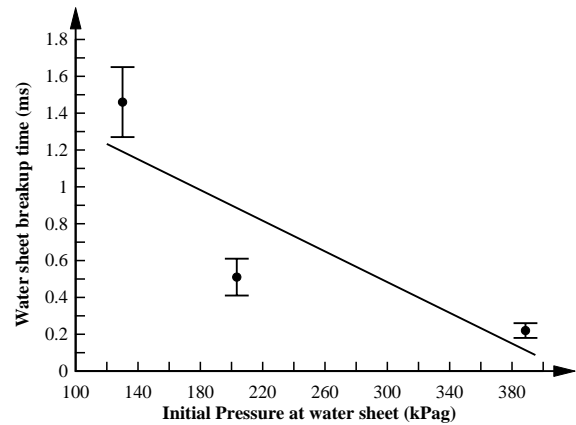


Fig. 5 Experimental breakup times of the water-sheet. The error bars represent the standard error between the three tests conducted. The solid line highlights the general trend of the data.

3.3 Role of the standoff distance

Three different standoff distances are considered, such that as the standoff distance increases the water-sheet is loaded by a comparatively weaker blast wave. Regardless, the velocity of the transmitted wave is approximately sonic in all cases, and it is found that the initial peak overpressure is approximately the same. Based on this observation alone, one could conclude that the standoff distance has a minimal effect on the transmitted wave. However, as discussed in the previous section for the conditions considered here, the transmitted sonic wave is followed by a large second rise in pressure caused by passage of the reaction products. To determine if this second rise in pressure can be minimized, the physical mechanisms are analyzed in more detail.

3.4 Shadowgraphy visualization

The shock wave interaction with the water-sheet is visualized using shadowgraphy. Select images from a high-speed shadowgraphy video are shown in Fig. 6, where the flow is right to left. The video is taken without pressure gauges which tend to obstruct the observation of the incident, reflected, and transmitted shock waves. The reflected wave seen in the third image is due to the impedance differences between the air and water [11]. In the fourth image a weak transmitted shock wave is observed.

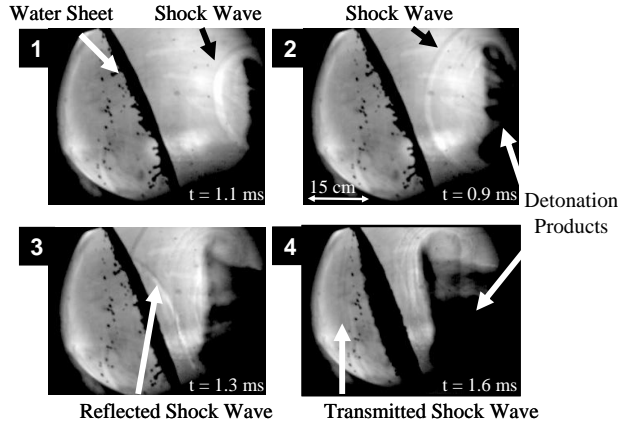


Fig. 6 High speed shadowgraphy of a blast loaded water-sheet at a 31 cm standoff distance.

The shadowgraphy images were compared to the pressure traces and were found to be in agreement. The last image in Fig. 6 shows the initial transition of a shock wave and change in water-sheet geometry. In agreement with the pressure readings, velocity estimates from the high speed videos indicate that the large cloud of detonation products travels at speeds below sonic conditions.

4 Numerical simulation using CTH

Numerical simulations were completed utilizing Sandia's hydrocode, CTH. CTH is a multi-material, large deformation, strong shock wave, solid mechanics code developed at Sandia National Laboratories [12]. In what follows, the CTH model is first validated using the free field conditions and is then used to qualitatively study the interaction of the shock wave and water-sheet.

4.1 Model geometry and boundary conditions

An axisymmetric model of a shock tube with a 3 gram charge of Primasheet 1000, similar to the experimental configuration, was first attempted. Results demonstrated a direct dependence between the shape and placement of the explosive charge and the simulated pressure at the exit of the shock tube. In addition, CTH did not demonstrate the pulse width increasing effect observed in previous shock tube experiments [8, 9]. This led to the development and use of an open field charge model.

The model developed and compared to the experimental results is shown in Fig. 7. The model is axisymmetric with a spherical open field charge of PETN. The bottom boundary condition is set to allow

the pressure to be zero in the ghost cells and to later remove all material from that ghost cell. This boundary condition ensures that mass does not enter the mesh but is allowed to leave. The remaining three boundary conditions use a sound speed based absorbing/transmitting condition to approximate an infinite or semi-infinite medium. Here mass can flow into and out of the mesh.

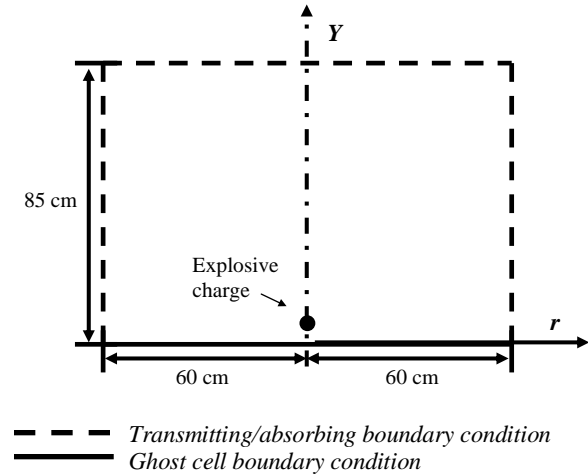


Fig. 7 CTH simulation geometry and boundary conditions.

4.2 Material equations-of-state

The explosive charge is assumed to follow the Jones–Wilkins–Lee (JWL) equation-of-state (EOS) for PETN. Since the experimental explosive is comprised of 63% PETN, the model mass is scaled to allow the use of the JWL EOS. The explosive charge is detonated using a history variable reactive burn (HVRB) model. The HVRB is a pressure-based model used to treat shock induced initiation that grows to a detonation for heterogeneous explosive material [13]. When the HVRB is used, the equations of state for the un-reacted and reacted phases are usually the Mie–Grüneisen and JWL equations of state [13]. Atmospheric air was modeled at an initial absolute pressure of 100 kPa using a tabulated SESAME EOS. The SESAME EOS Library is a standardized, computer-based library of thermodynamic properties developed by Los Alamos [14].

4.3 Comparison to free field experiments (without water-sheet)

Fixed nodes are included in the CTH model to match the experimental free field pressure gauge locations. The mass of PETN used in the model (48.4 grams) was determined by comparing the predicted pressure

to the experimental pressures and adjusting the mass until reasonable agreement was obtained. It should be noted that the mass of the PETN used in the model is an order of magnitude larger than the experiment value. This difference can be attributed to the fact that a shock tubes is used in the experiment to focus the blast in one direction. Figure 8 compares the free field pressure traces between the final CTH model and the experimental results. The average percent difference between the peak overpressure is 7.8% and the average percent difference between the impulses is around 20%.

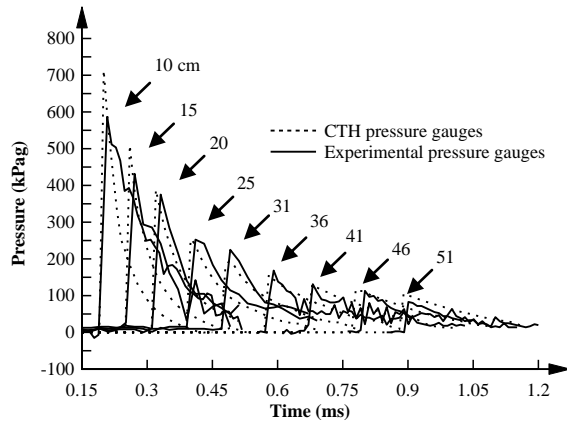


Fig. 8 Comparison of CTH pressure traces vs. experimental pressure traces. Numbers indicate the distances in cm between the exit of the shock tube and the pressure gauge.

4.4 Modeling the water-sheet in CTH

Modeling the 0.3 cm thick water-sheet requires a fine mesh. The meshing style is a fixed Eulerian mesh, where the materials flow through the fixed mesh. The mesh consisted of 24,000 and 17,000 nodes in the x- and y-direction, respectively. This resulted in a structured mesh, with meshing cells being $\frac{1}{2}$ mm by $\frac{1}{2}$ mm. A convergence study was performed to show that the solution was not dependent on mesh refinement.

Liquid water is modeled with the Mie-Grüneisen EOS. In simulations where the surface of the water-sheet is assumed to be initially smooth, sheet breakup and the transmission of a second pressure rise is not observed. However, as mentioned in the experimental section, the actual water-sheet displays visible surface roughness. Therefore, it is desired to determine what effect this roughness has on the fragmentation process. To do so, several test cases are considered in which the surface of the water sheet is modeled using a sine wave with different spatial frequencies. Comparisons of the water-sheet geometries are shown in Fig. 9. In all cases, the thickness of the water sheet

varies between 0.3 cm and 0.1 cm, and all geometries contain the same total mass (cross-sectional area). The water-sheets are also assumed to be infinite (stretching across CTH domain) to eliminate effects caused by diffraction of the shock wave around the water-sheet, and to better isolate the interaction of the shock wave and water-sheet. In addition, it should be noted that the CTH models do not include surface tension effects which may play a significant role in the physical breakup process. Because of these simplifications, the simulation results are considered for qualitative insight into the physical phenomena, rather than quantitative predictions.

As expected, varying these perturbations affects the breakup time and the magnitude of the transmitted shock wave. Results presented in the remainder of this work are calculated assuming an initial perturbation given by case (D) in Fig. 9, as this case shows the best qualitative agreement with the experimental results.

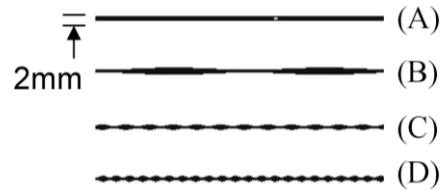


Fig. 9 (A) Straight 2 mm thick water-sheet, (B) water sheet with a wavelength of 50 mm, (C) water sheet with a wavelength of 8.3 mm, and (D) water sheet with a wavelength of 4.2 mm. *NOTE: All the water sheets with perturbations are between 0.3 cm and 0.1 cm thick.*

4.5 Water sheet simulation results and comparisons

Figure 10 shows a comparison of the CTH model and experimental results at 5 and 10 cm after the water-sheet at a 20 cm standoff distance. Both the experimental and numerical results show an initially transmitted pressure wave and a later second pressure rise. To highlight the physical processes, Fig. 11 shows predicted contours of pressure at select time intervals. Due to the impedance mismatch at the air-water interface, a significant portion of the initial shock reflects off the water-sheet and only a weak shock wave is initially transmitted. However, as observed in experiments, the water-sheet eventually fragments, and consequently the high pressure detonation products are released, causing the observed second rise in pressure.

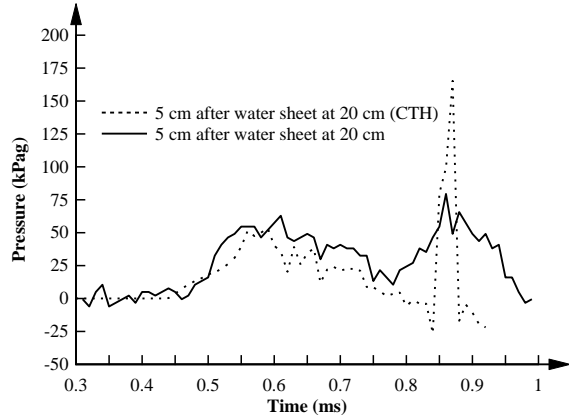


Fig. 10 Comparison between CTH and experimental pressure traces 5 cm after the water-sheet at a 20 cm standoff distance.

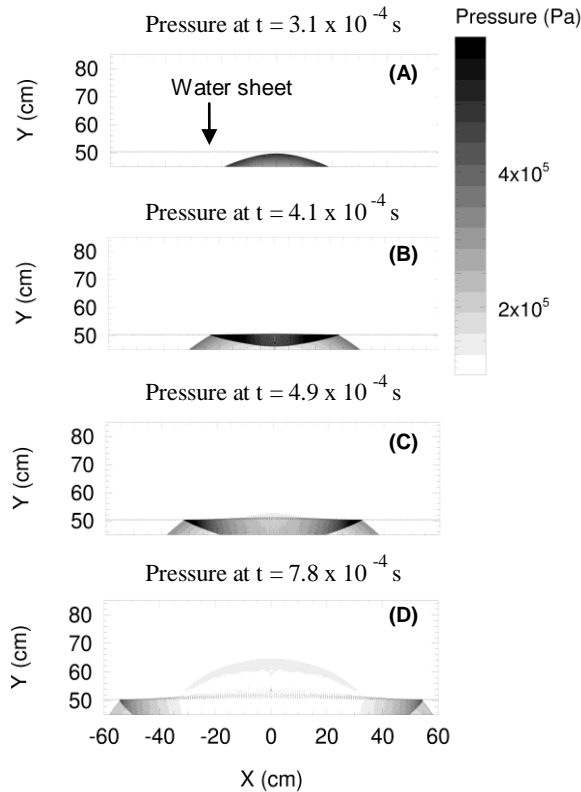


Fig. 11 Simulation results showing absolute pressure for shock wave interaction with the water-sheet at the 20 cm standoff distance. (A) initial shock wave reaches the water-sheet, (B) reflection of a shock wave off the surface of the water-sheet, (C) development of weak transmitted shock wave behind the intact water-sheet, and (D) water-sheet breakup and transition of pressure wave.

5 Discussion

Figure 12 highlights the general form of the transient overpressure observed in experiments and simulations. As discussed by Henderson et al. [11], when a blast wave first contacts a water-sheet, a large portion of the incident energy is reflected back towards the source due to the impedance mismatch at the air-water interface. The remaining energy, which is transmitted through the water-sheet, forms the observed weak shock wave and the resulting initial pressure rise. For the experimental conditions considered here, the initial blast peak overpressure is mitigated by as much as 80%. However, a second rise in pressure is observed, resulting in a much greater overpressure behind the water-sheet. If a mechanism is available to prevent this second pressure rise, a water-sheet may be an effective emergency blast mitigant.

High speed shadowgraphy (Fig. 6) and simulations (Fig. 11) confirm that the second rise in pressure is due to the breakup of the water-sheet and the passage of the detonation products. When the blast wave initially reflects off the water-sheet, a large pressure differential exists between forward and back surfaces of the water-sheet (see Fig. 11). It is well known that pressure differentials of this nature give rise to surface instabilities which grow and eventually lead to fragmentation. This process takes a finite time, referred to as the breakup time (Fig. 5). It should also be noted that the pressure differential across the water-sheet decreases with time due to the propagation of the reflected shock wave away from the water-sheet. Therefore, water-sheet fragmentation may be prevented if the characteristic breakup-time is sufficiently longer than the time required for dissipation of the pressure differential across the water-sheet.

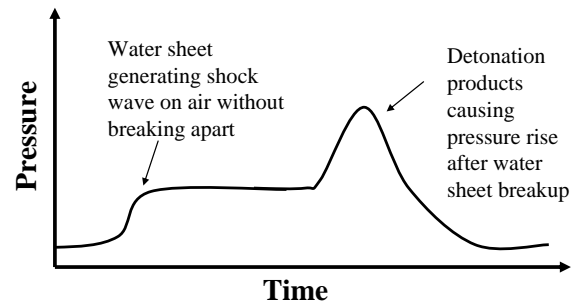


Fig. 12 Typical pressure trace of water-sheet breakup under shock loading.

A few methods are available to increase the effective breakup time of a water-sheet. (1) To the extent possible, the surface of the water-sheet should be free from initial perturbations; (2) the thickness of the water-sheet can be increased; and/or (3) multiple water-sheets can be utilized. The effectiveness of method (1) is confirmed by the simulation results presented in the previous section. However, this method may be difficult to implement due to the capillary instability and water-sheet turbulence. Methods (2) and (3) have been shown to increase blast mitigation in previous investigations [4-6] and were also qualitatively investigated using the CTH model discussed in the previous section. The details of those simulations are omitted for conciseness. However, the conclusions are consistent with the previously published work. Further quantitative experiments and simulations are needed to confirm these results.

5 Conclusions

An experimental investigation of blast mitigation using a 0.3 cm thick water-sheet is presented. Results show an initially decreased peak overpressure and impulse regardless of water-sheet standoff distance. This initial mitigating potential agrees qualitatively with previous literature.

A numerical model using CTH is developed and validated with the free-field experimental data. In simulations with a water-sheet, an initial pressure rise results from the passage of a low pressure shock wave ($M \approx 1$) through the intact sheet and into the air behind it. Following this, the water-sheet breaks apart due to an increase in pressure on the forward surface caused by the buildup of the subsonic detonation products. Passage of the detonation products after breakup results in a large second rise in pressure behind the water-sheet. Additionally, the numerical model along with experimental shadowgraphy reveal that water sheet breakup follows a multi-step process. The water sheet breakup time was found to be a function of the perturbation in the water sheet. In addition, from experimental and numerical results the water-sheet breakup time decreases with increasing strength of the incident shock wave.

The water-sheet is shown to be advantageous for mitigating an incident blast wave if sheet breakup can be prevented or delayed. A few possible methods are proposed and further experimental and numerical investigations are needed to confirm their validity.

Acknowledgements We would like to thank the Department of Homeland Security and the Center of

Excellence for Explosive Detection, Mitigation and Response, Sponsor Award No. 080409/0002251. We would also like to thank Justin Wagner for his technical review of this paper. Additionally, special thanks to Eric Miklaszewski, Matthew Massaro, and Jesus Mares who assisted with experiments.

Sandia National Laboratories is a multi-program laboratory managed and operated by Sandia Corporation, a wholly owned subsidiary of Lockheed Martin Corporation, for the U.S. Department of Energy's National Nuclear Security Administration under contract DE-AC04-94AL85000.

References

1. National Research Council: Protecting buildings from bomb damage: Transfer of blast-effects mitigation technologies from military to civilian applications. National Academy, Washington, DC (1995)
2. Kailasanath, K., Tatem, P. A., Williams, F. W., and Mawhinney, J.: Blast mitigation using water – A status report. NRL Memorandum Report, 6410-02-8606 (2002)
3. Schwer, D., Kailasanath, K.: Blast Mitigation by Water Mist (3) Mitigation of Confined and Unconfined Blasts. NRL Memorandum Report, 6410-06-8976, (2006)
4. Cheng, M., Hung, K. C., and Chong, O. Y.: Numerical Study of Water Mitigation Effects on Blast Waves. Shock Waves 14, 217-223 (2005)
5. Shin, Y. S., Lee, M., Lam, K. Y., Yeo, K. S.: Modeling mitigation effects of water shield on shock waves. Shock Vib. 5, 225–234 (1998)
6. Meekunnasombat, P., Oakley, J.G., Anderson, M.H., Bonazza, R.: Experimental study of a shock-accelerated liquid layer. Shock Waves 15, 383-397 (2006)
7. Bremond, N., Villermaux, E.: Bursting thin liquid films. J. Fluid Mech. 524:121–30 (2005)
8. Freiwald, D. A.: Approximate blast wave theory and experimental data for Shock trajectories in linear explosive driven shock tubes. Jpn. J. Appl. Phys. 43, 2224-2226 (1972)
9. Alley, M. D.: Explosive Blast Loading Experiments for TBI Scenarios: Characterization and Mitigation. Thesis. West Lafayette, IN / Purdue University, (2009)
10. Settles, G.: High-speed imaging of shock waves, explosives, and gunshots. Am. Sci. 94, 22-31 (2006)
11. Henderson, L. F., Ma, J. H., Sakurai, A., Takayama, K.: Refraction of a shock wave at an air-water interface. Fluid Dynamics Res 5, 337-350 (1990b)
12. Crawford, D.: CTH Shock Physics. Sandia National Laboratories. <http://www.sandia.gov/CTH/> (2012). Accessed 14 Dec. 2011
13. Todd, S. N., Anderson, M. U., Caipen, T. L.: Modeling for non shock initiation. Dynamic Behav. of Mater. 1, 179-186 (2011)
14. Lyon, S. P., Johnson, J. D.: SESAME." The Los Alamos National Laboratory Equation of State

Database. Equation of State and Mechanics of
Materials (T-1), LANL.
http://t1web.lanl.gov/doc/SESAME_3Ddatabase_se_1992.html (1992). Accessed 10 Nov. 2011

Figure 1
[Click here to download high resolution image](#)

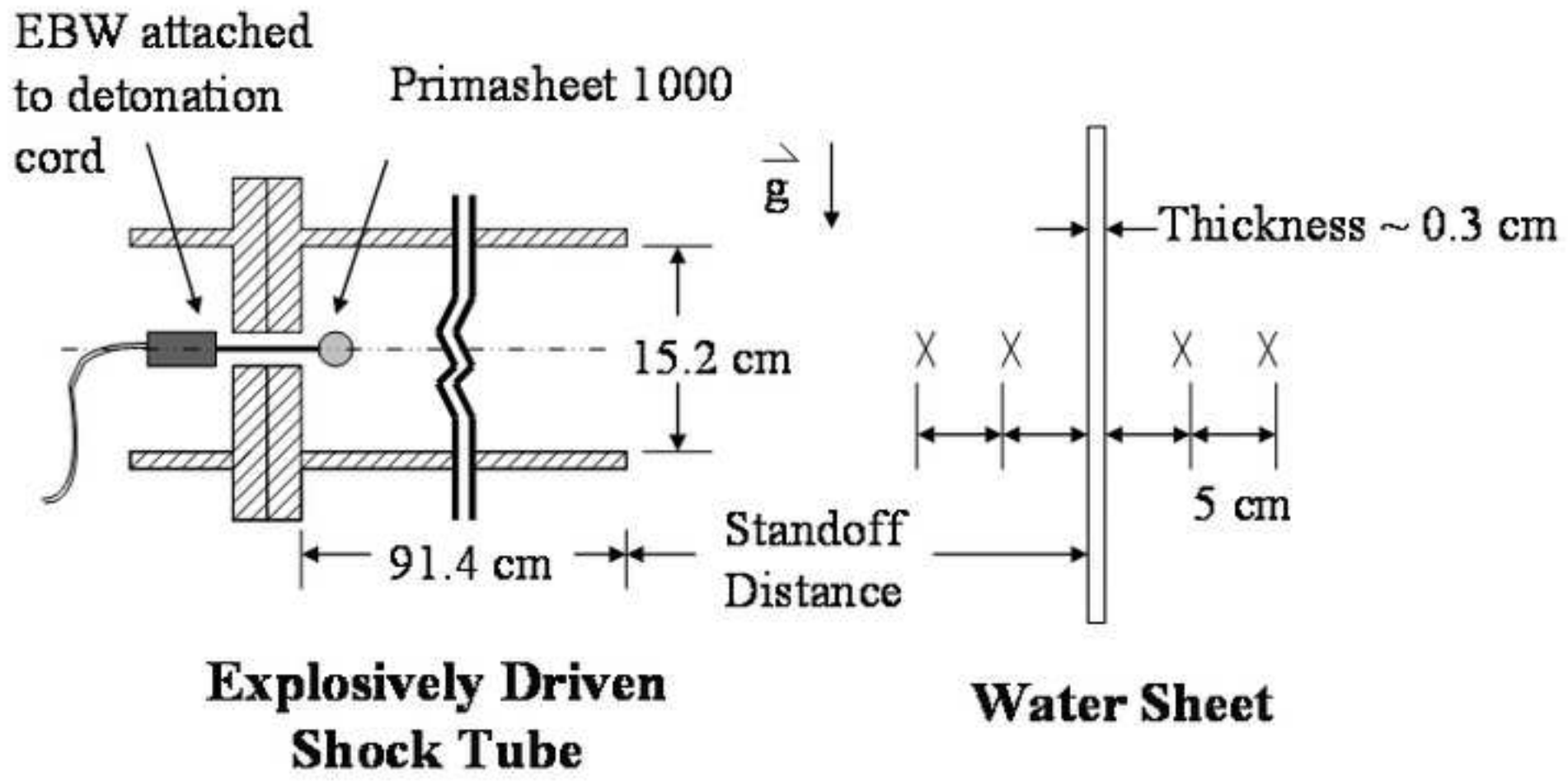


Figure 2
[Click here to download high resolution image](#)

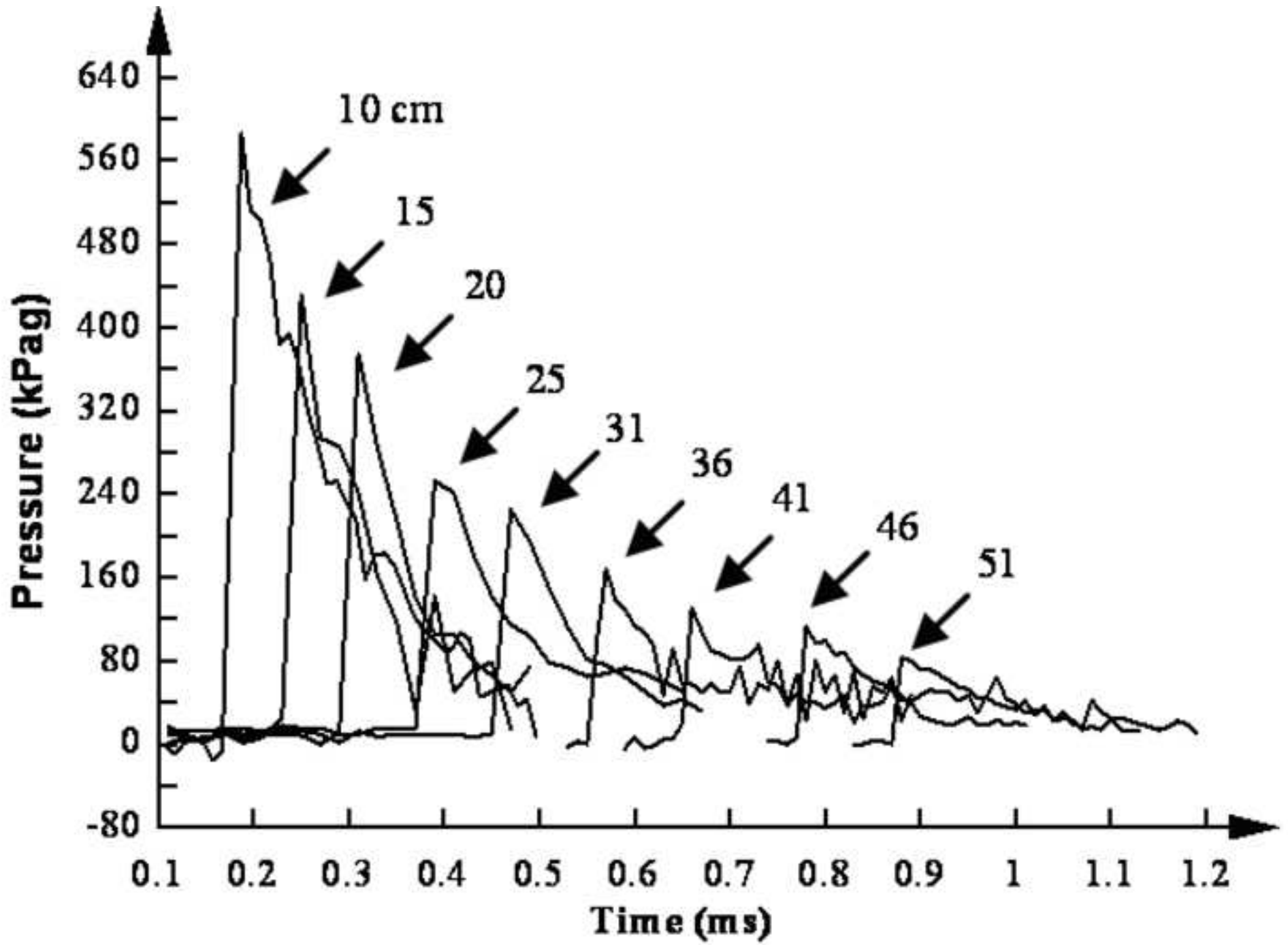


Figure 3
[Click here to download high resolution image](#)

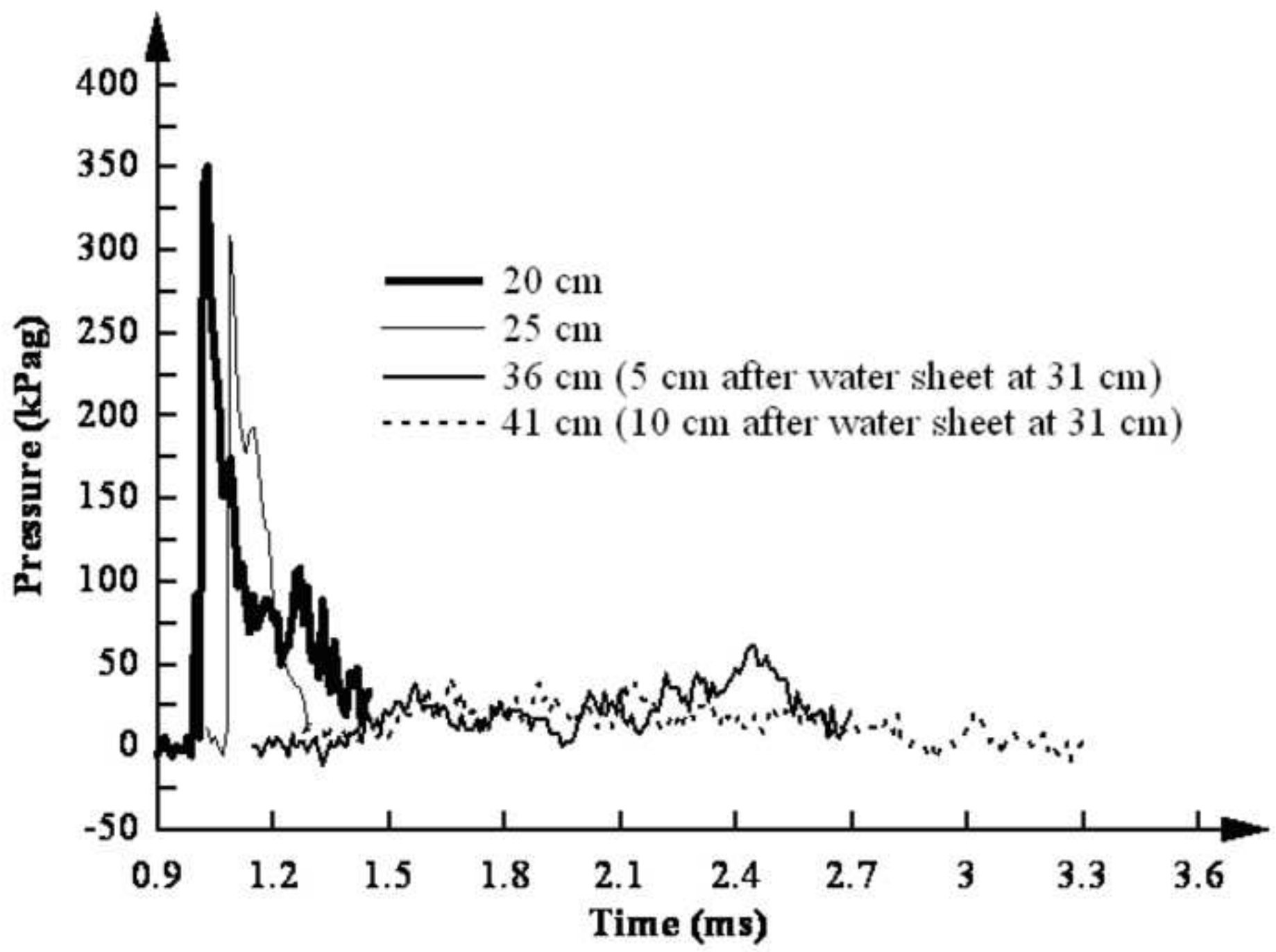


Figure 4
[Click here to download high resolution image](#)

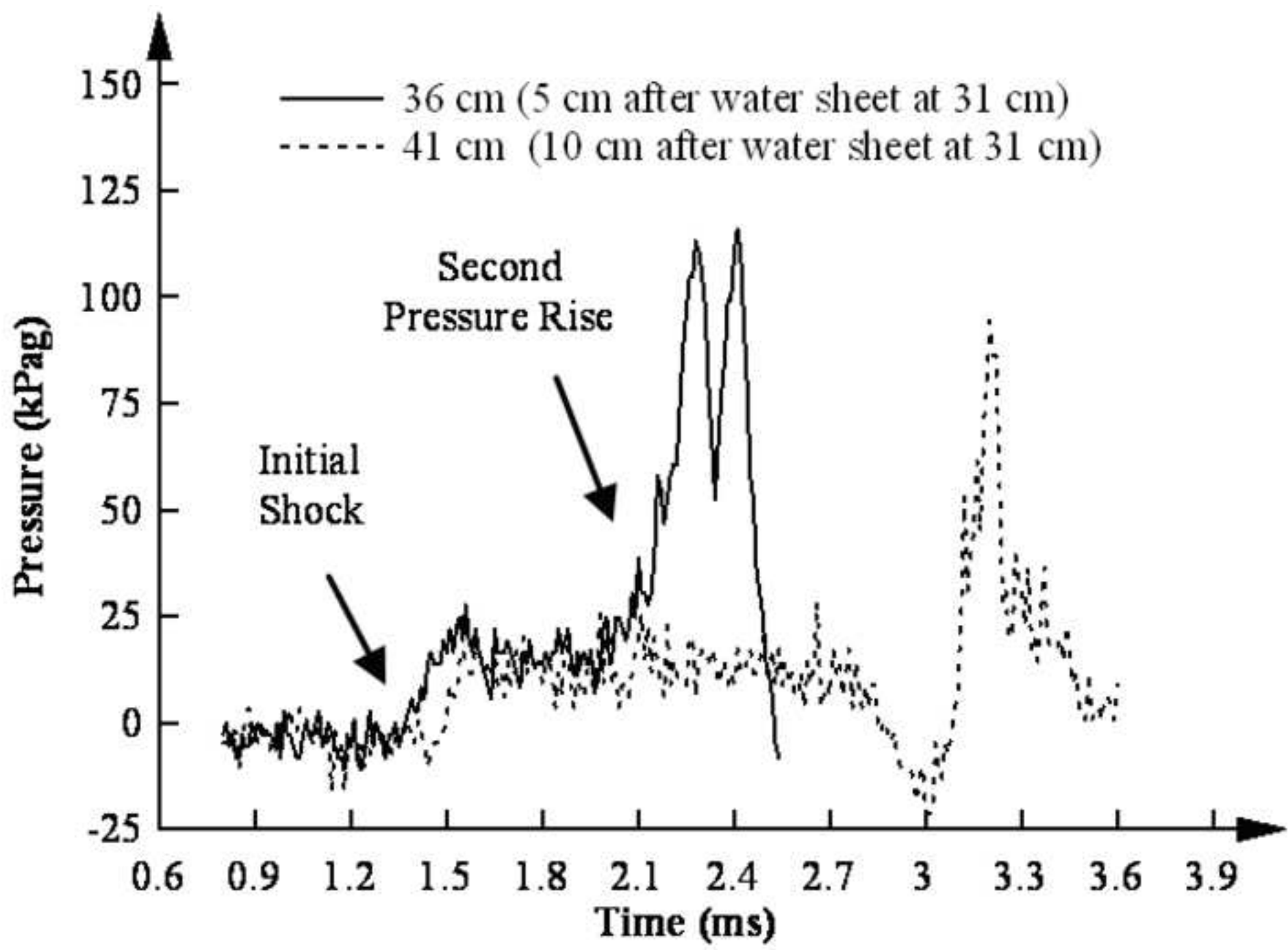


Figure 5
[Click here to download high resolution image](#)

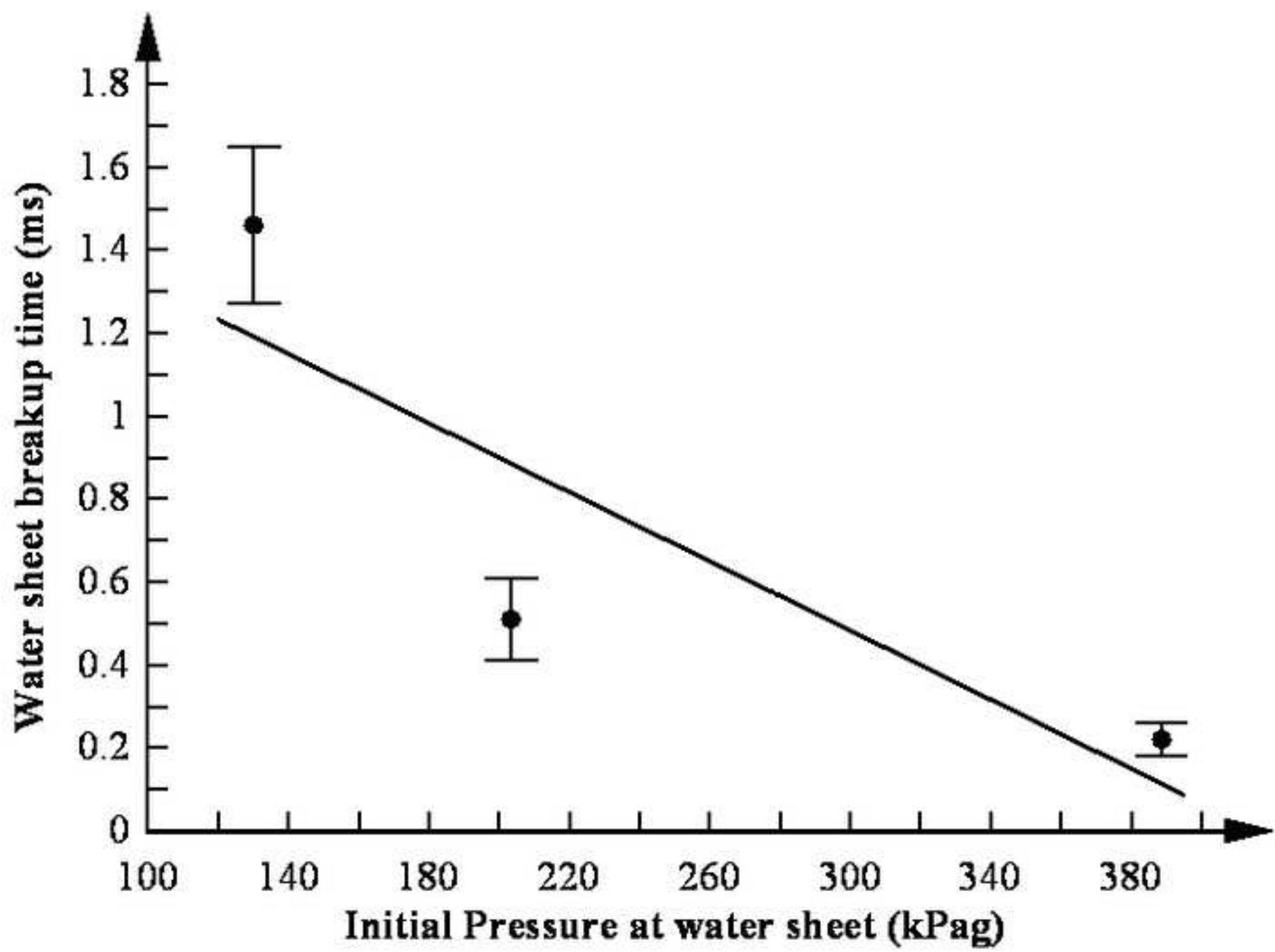


Figure 6
[Click here to download high resolution image](#)

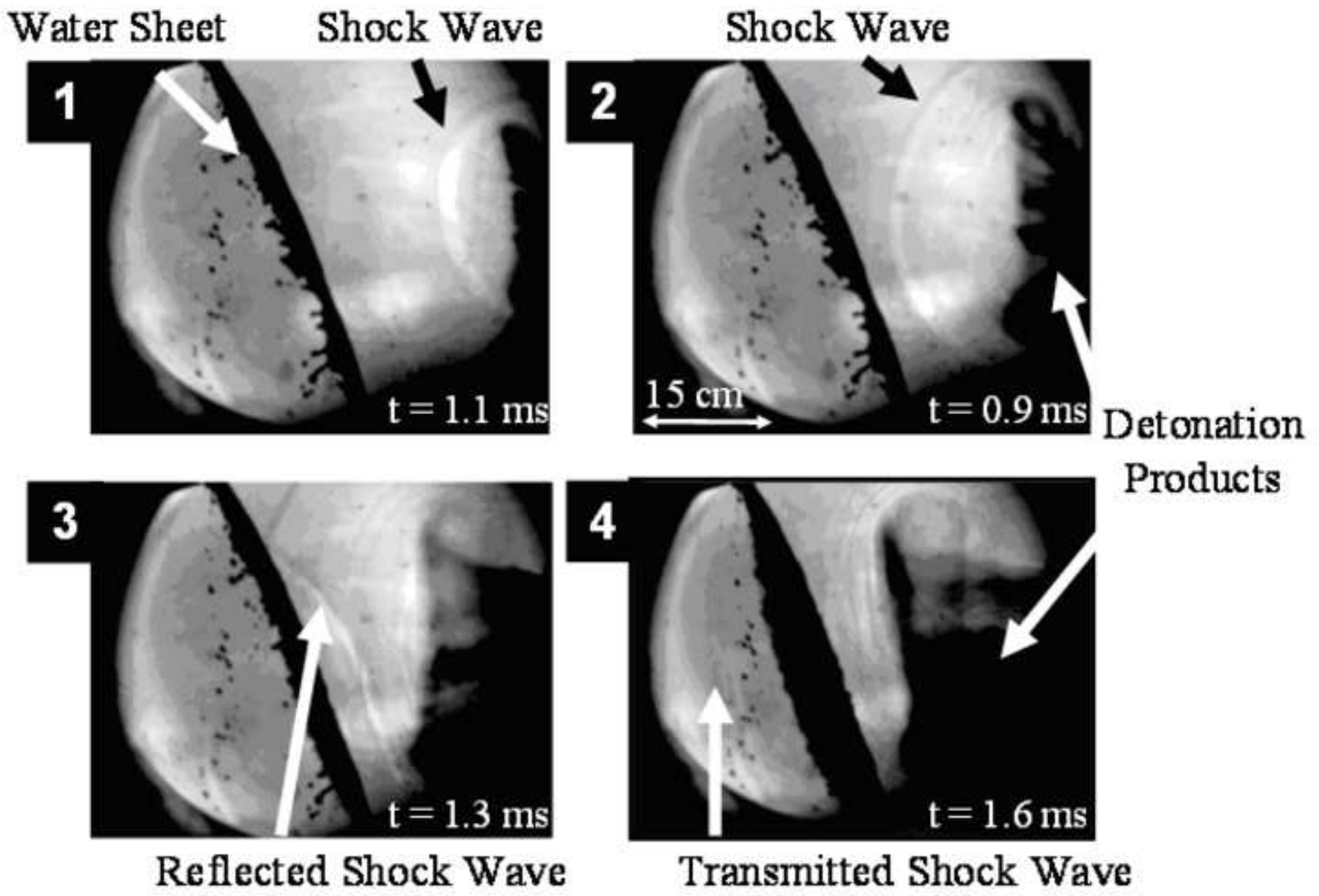
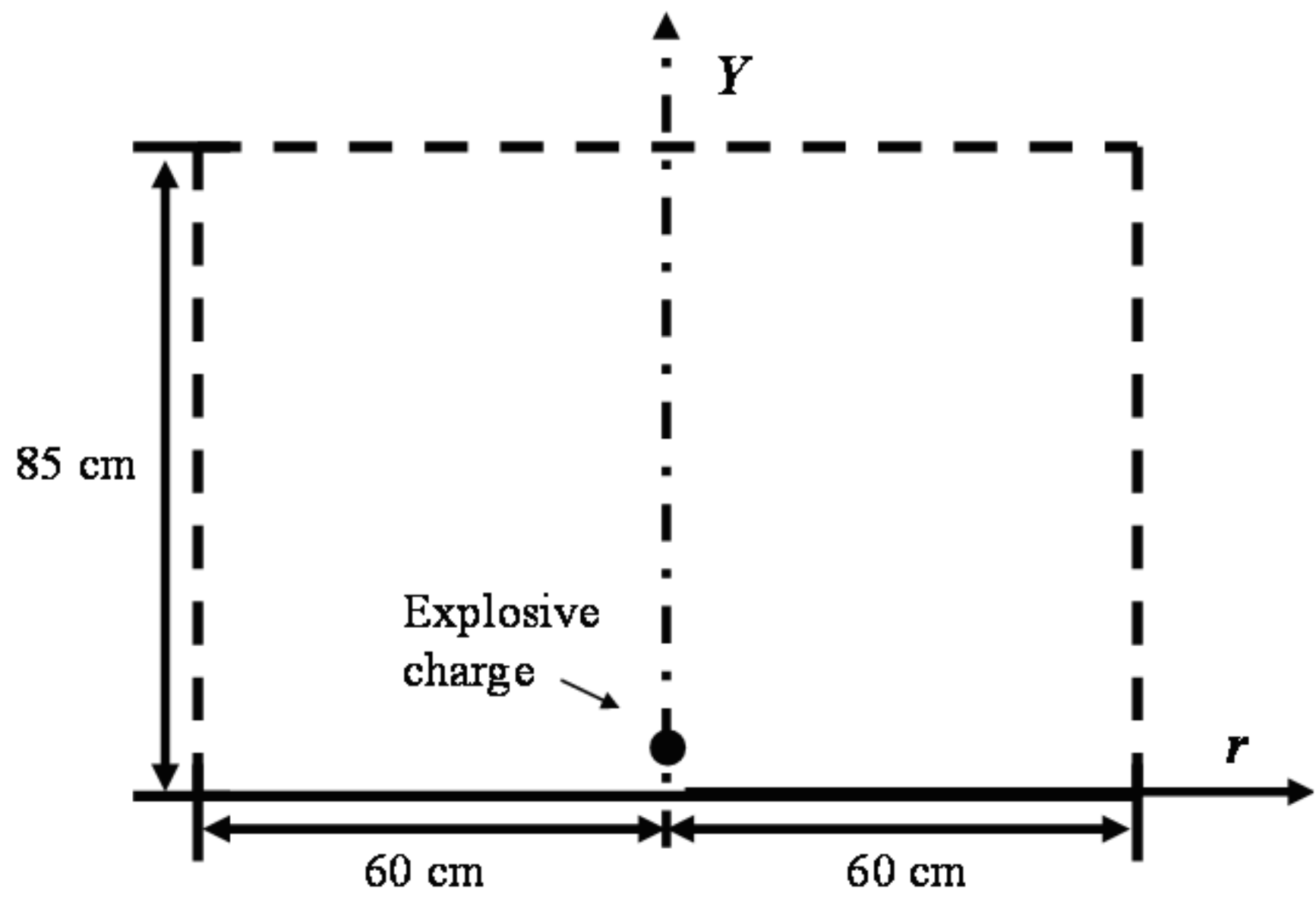
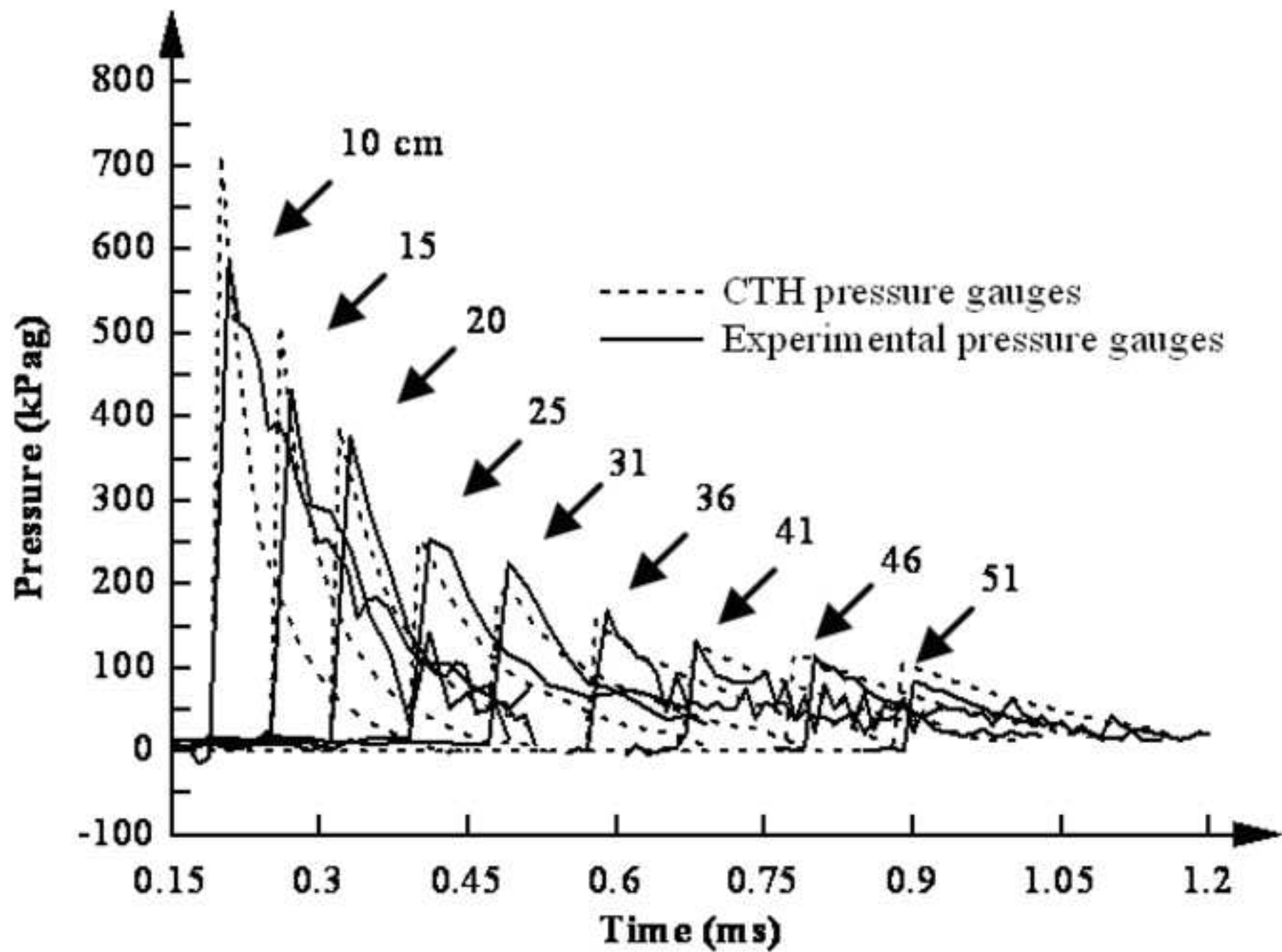


Figure 7
[Click here to download high resolution image](#)



- - - *Transmitting/absorbing boundary condition*
———— *Ghost cell boundary condition*

Figure 8
[Click here to download high resolution image](#)



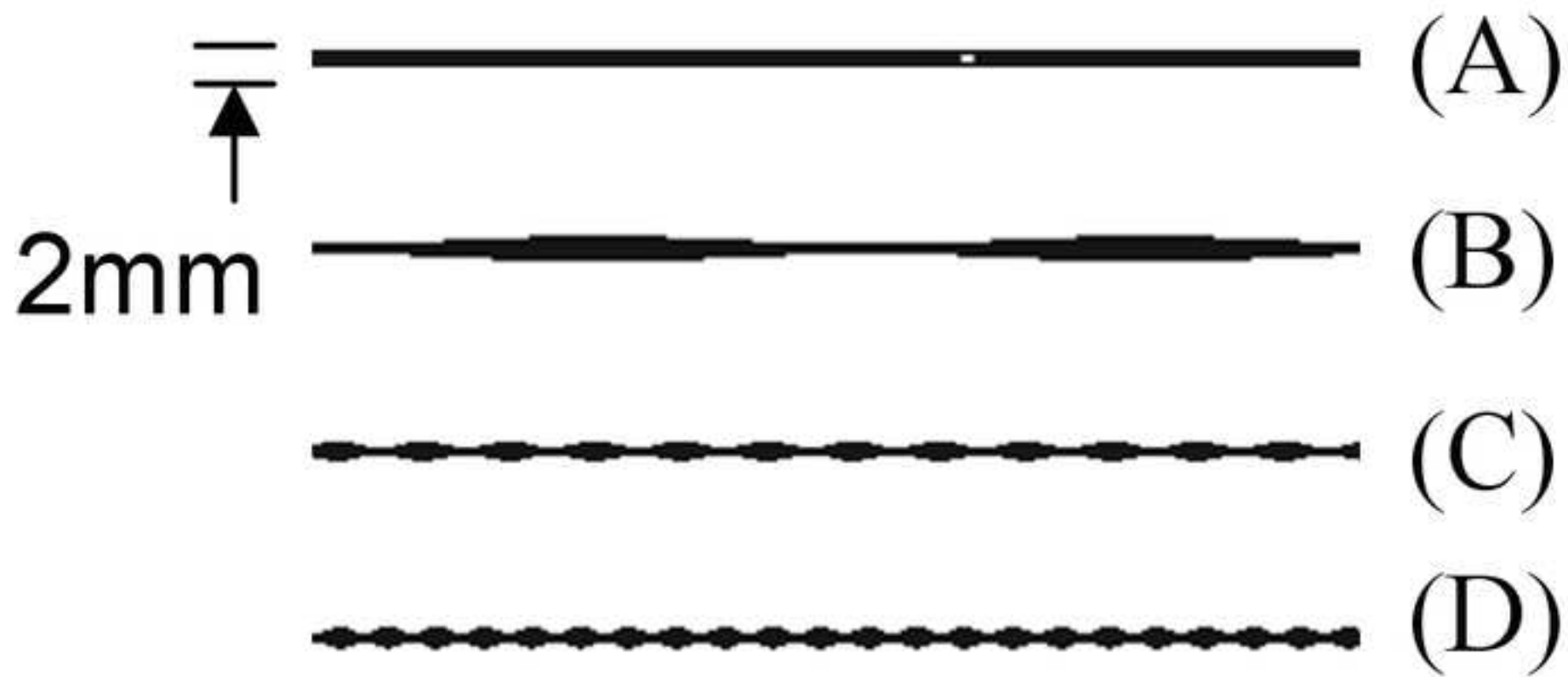


Figure 10
[Click here to download high resolution image](#)

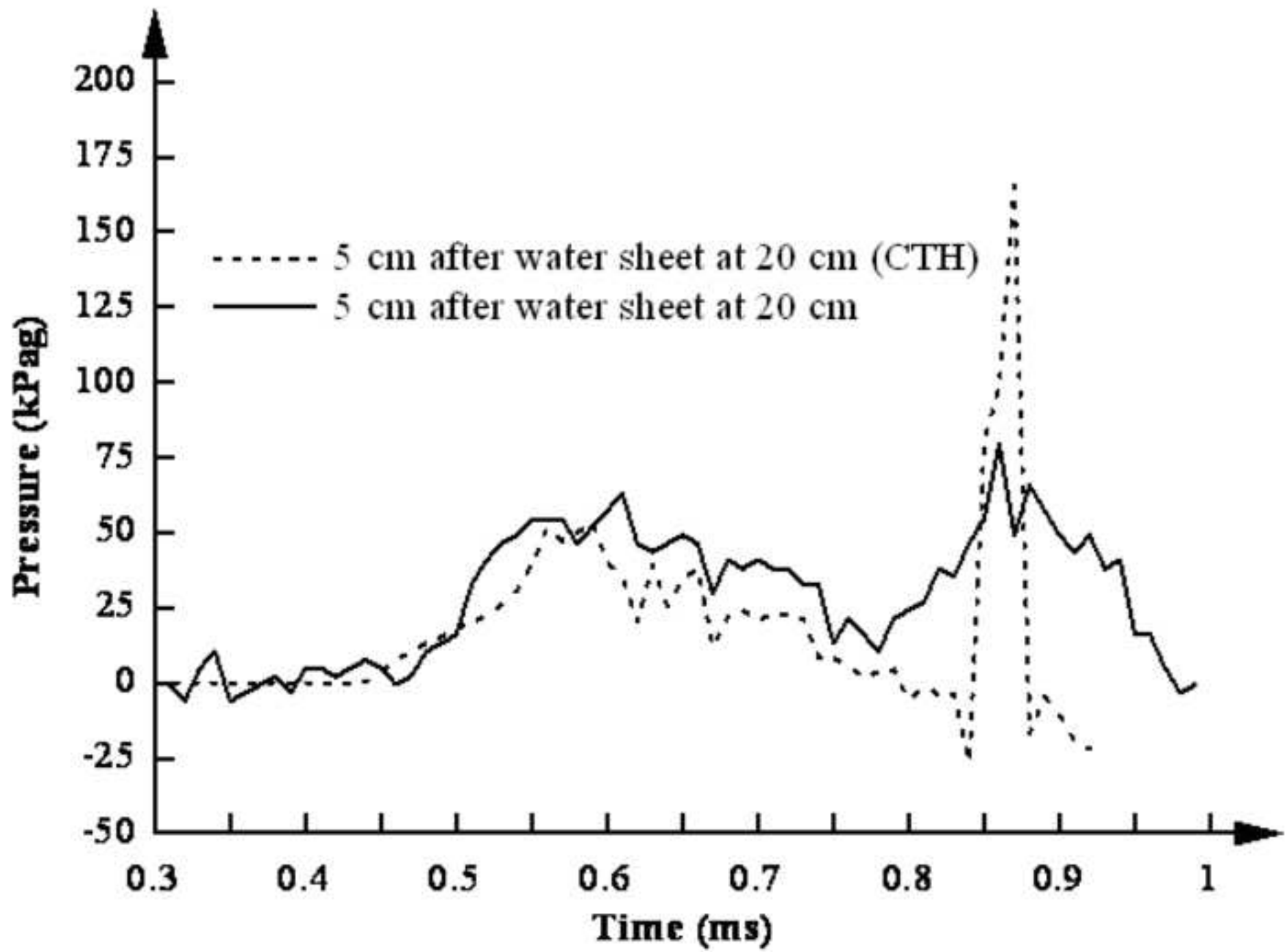


Figure 11
[Click here to download high resolution image](#)

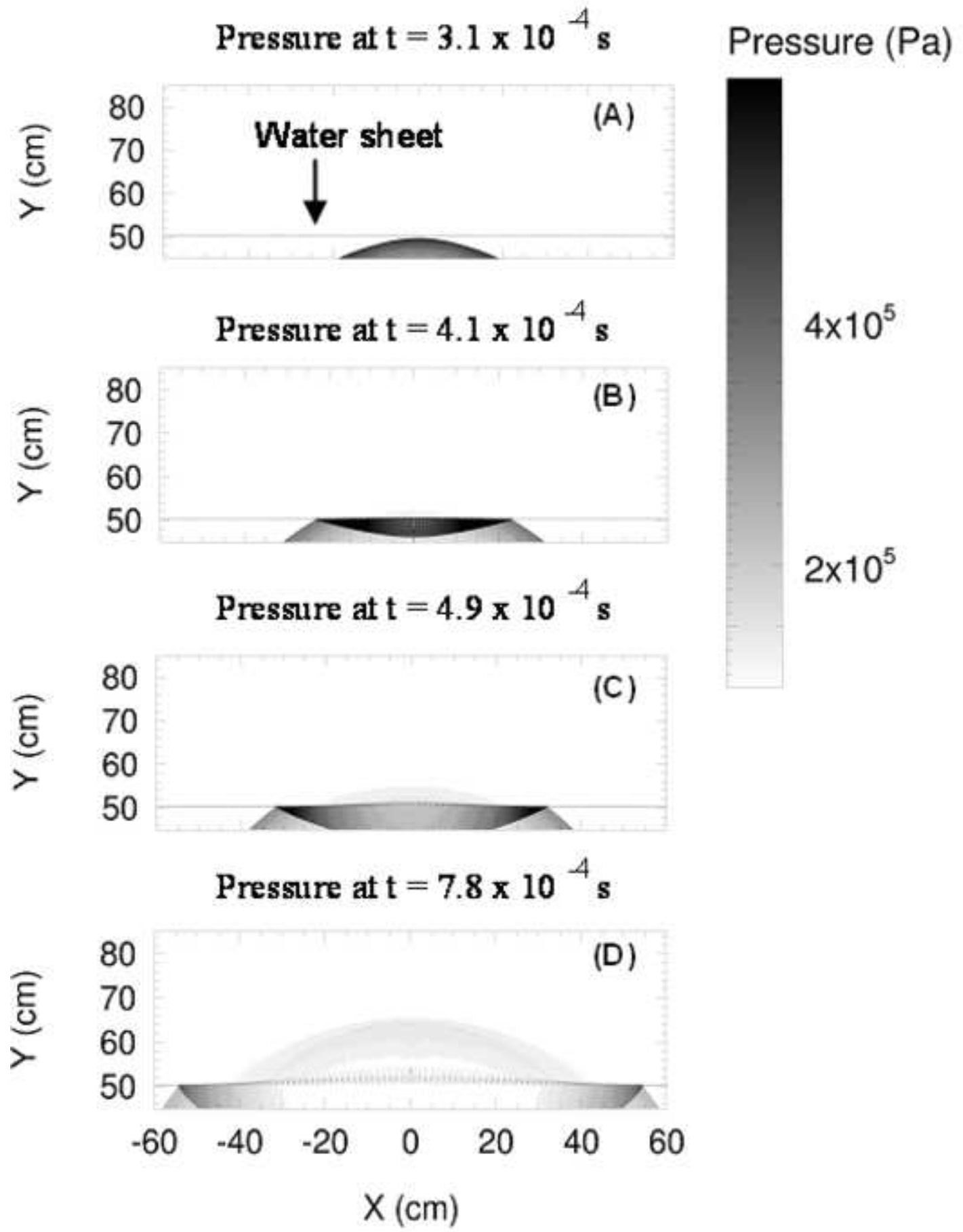


Figure 12
[Click here to download high resolution image](#)

